AGU ADVANCING EARTH AND SPACE SCIENCES

Geophysical Research Letters

RESEARCH LETTER
10.1029/2023GL106963

Key Points:

- Sea ice models exhibit higher (lower) basal thermodynamic growth in the central Arctic (peripheral seas) compared to observational estimates
- When summed, all other sea ice model effects are lower (higher) in the central Arctic (peripheral seas) compared to observational estimates
- Adjustment of dynamic effects closer to observational estimates would correct biases in mean thickness and basal thermodynamic growth

Supporting Information:

Supporting Information may be found in the online version of this article.

Correspondence to:

J. Anheuser,
jfanheus@ncsu.edu

Citation:

Anheuser, J., Liu, Y., & Key, J. (2024). Model mean state sea ice thickness reflects dynamic effect biases: A process based evaluation. *Geophysical Research Letters*, *51*, e2023GL106963. https://doi.org/10.1029/2023GL106963

Received 24 OCT 2023
Accepted 22 FEB 2024

Author Contributions:

Conceptualization: James Anheuser
Data curation: James Anheuser
Formal analysis: James Anheuser
Funding acquisition: Yinghui Liu, Jeff Key
Investigation: James Anheuser
Methodology: James Anheuser
Project administration: Yinghui Liu, Jeff Key
Software: James Anheuser
Supervision: Yinghui Liu, Jeff Key
Validation: James Anheuser
Visualization: James Anheuser
Writing – original draft: James Anheuser
Writing – review & editing: James Anheuser

Model Mean State Sea Ice Thickness Reflects Dynamic Effect Biases: A Process Based Evaluation

James Anheuser[1], Yinghui Liu[2], and Jeff Key[2]

[1]Cooperative Institute for Meteorological Satellite Studies, University of Wisconsin-Madison, Madison, WI, USA, [2]Center for Satellite Applications and Research, NOAA/NESDIS, Madison, WI, USA

Abstract Global climate models account for sea ice thickness by summing thermodynamic processes that affect thickness through phase change and dynamic processes that affect thicknesses through relative motion. Comparison of these individual processes with observations is essential for model interpretation and development. We utilized observational estimates of basal thermodynamic growth, overall thickness changes and their residual difference (including dynamics) to evaluate these processes in the National Center for Atmospheric Research (NCAR) Community Earth System Model 2 (CESM2) submission to the World Climate Research Program (WCRP) Ocean Model Comparison Project Phase 2 (OMIP2) and Pan-Arctic Ice–Ocean Modeling and Assimilation System (PIOMAS). Both models exhibit a similar pattern of higher basal thermodynamic growth and lower residual effects and wintertime thickness in the central Arctic than observational estimates for 2010–2018, and vice versa in the peripheral seas. Correcting residual effect biases would ameliorate the biases in both mean thickness and basal thermodynamic growth.

Plain Language Summary Sea ice models include two types of processes. Those causing phase change, called thermodynamic processes and those causing thickness changes through relative motion of ice parcels, called dynamic processes. We compare the effects of these processes in two models to observational estimates to aid the interpretation of ice thickness in these models and drive development. We find that the biases in the dynamic effects drive biases in mean thickness and thermodynamic processes, which could in turn be reduced if dynamic components biases were to be improved.

1. Introduction

Global climate model simulation results are often used to project future Arctic sea ice conditions (Arthun et al., 2021; Arzel et al., 2006; Flato & Participating CMIP Modelling Groups, 2004; Lebrun et al., 2019; Smith & Stephenson, 2013; Wang & Overland, 2015). Within these climate models, sea ice models account separately for thermodynamic and dynamic processes to predict how the ice will respond in a changing climate (Hibler, 1980; Thorndike et al., 1975; Zhang & Rothrock, 2001). Comparison of observed and model predicted conditions is essential to building confidence in these predictions. Processes that contribute to key outputs must also be compared against observations. This is especially important given that the individual processes contributing to a key variable may be affected by differing mechanisms in a changing climate, as is the case with dynamic and thermodynamic sea ice processes.

Sea ice model output has been compared against available observations (Boe et al., 2009; Massonnet et al., 2012; Notz et al., 2020; Shu et al., 2015, 2020; Stroeve et al., 2007). While the mass budget of sea ice has been explored (Holland et al., 2010; Keen et al., 2021), absent is comparison of modeled thermodynamic and dynamic sea ice thickness effects independently against observations. The primary reason for this has been a lack of such observations. Allowing such a comparison, Anheuser et al. (2023a) presents a monthly, Arctic-basin-wide, and 25 km resolution Eulerian estimation of thermodynamic thickness growth occurring at the ice–ocean interface, called basal thermodynamic growth, and the difference between this growth and overall thickness change, called residual thickness effects, on wintertime sea ice thickness from 2010 to 2021.

Here, mean overall thickness, basal thickness growth and residual thickness effects from the National Center for Atmospheric Research (NCAR) Community Earth System Model (CESM2) submission to the Ocean Model Intercomparison Project Phase 2 (OMIP2) and Pan-Arctic Ice Ocean Modeling and Assimilation System (PIOMAS) are compared to Alfred Wegener Institute (AWI) CryoSat-2/Soil Moisture and Ocean Salinity (CS2SMOS) sea ice thickness and the observational estimates from Anheuser et al. (2023a), created using the

Stefan's Law Integrated Conducted Energy (SLICE) method (Anheuser et al., 2022). Because both CESM2-OMIP2 and PIOMAS are reanalysis-forced, their outputs should closely represent the conditions that occurred during a given historical time period. Any observed deviations from these conditions can be used for model interpretation and improvement.

2. Data

Both CESM2-OMIP2 and PIOMAS output thermodynamic sea ice thickness growth terms and a dynamic sea ice effect term that are similar to the observational estimates shown in Anheuser et al. (2023a), within whose framework these two processes sum to overall growth via the following governing equation:

$$\frac{\partial H}{\partial t} = f(t, H, \mathbf{x}) - \nabla \cdot (\mathbf{u}H), \tag{1}$$

where H is plane slab thickness; t is time; f is a function of time, thickness and position vector $\mathbf{x}$ describing thermodynamic thickness change; and $\mathbf{u}$ is the ice motion vector. The second term on the right hand side represents dynamic thickness processes. CESM2-OMIP2 and PIOMAS utilize a similar governing equation, characterizing thickness as a distribution discretized into bins rather than a slab thickness and including a ridging term to transfer volume between bins as described by Thorndike et al. (1975).

2.1. AWI CS2SMOS

Sea ice thickness observations from satellite-based altimetry, such as those from European Space Agency (ESA) CryoSat-2 carrying the SAR/Interferometric Radar Altimeter-2 (SIRAL-2) instrument, have relatively high spatial resolution but low coverage owing to the small instrument footprint (Laxon et al., 2013; Wingham et al., 2006). At lower latitudes, these issues worsen as revisit times lengthen and uncertainties become larger as the ice thins. To address this issue, the AWI CS2SMOS thickness dataset combines thickness observations from CryoSat-2 with thickness retrieved using the ESA Soil Moisture and Ocean Salinity (SMOS) satellite, aboard which the Microwave Imaging Radiometer using Aperture Synthesis (MIRAS) instrument measures passive microwave brightness temperatures that are used along with a energy budget model to estimate thickness (Ricker et al., 2017). Through optimal interpolation, CS2SMOS reduces biases for thinner ice when compared against airborne NASA Operation Ice Bridge (OIB) data and more importantly provides weekly coverage of the entire Arctic basin on a 25 km EASE-Grid 2.0 by virtue of SMOS's daily basin-wide coverage.

2.2. SLICE

Observational estimates of sea ice thickness changes from basal thermodynamics and residual processes for comparison here were taken from Anheuser et al. (2023a), who used SLICE (Anheuser et al., 2022) to retrieve basal thermodynamic growth and calculate residual process effects, referred to henceforth as SLICE residual and defined as the difference between the retrieved thermodynamic growth and thickness changes from CS2SMOS sea ice thickness. These residual effects include primarily dynamic process changes but also include thermodynamic processes other than basal growth such as frazil growth, snow–ice formation or melt.

SLICE treats wintertime sea ice as a simple system exhibiting a linear vertical temperature profile between boundary condition temperatures at the ice–ocean interface and snow–ice interface. This relationship is described by Stefan's Law (Lepparanta, 1993; Stefan, 1891):

$$f(t, H, \mathbf{x}) = \frac{\kappa_{eff}}{\rho_i L H}\left(T_f - T_{si}\right) - \frac{F_w}{\rho_i L}, \tag{2}$$

where $f(t, H, \mathbf{x})$ is the thermodynamic growth rate, ρ_i is the density of sea ice, L is the latent heat of fusion, κ_{eff} is the effective thermal conductivity of sea ice, H is sea ice thickness, T_f is the freezing point of sea water, T_{si} is the snow–ice interface temperature, and F_w is basal heat flux from the liquid sea water to the solid sea ice. In SLICE, a passive microwave snow–ice interface temperature retrieval (Kilic et al., 2019) and CS2SMOS are inserted into this relationship to determine the thermodynamic growth rate. The multi-phase effects on latent heat of fusion and effective thermal conductivity are variable and accounted for using the relationships developed in Feltham

10.1029/2023GL106963

et al. (2006). Sea ice density and basal flux are set constant at 917 kg m^{-3} and 2 W^{-2}, respectively. Horizontal heat conduction, thermal inertia and internal heat sources are assumed to be negligible, limiting its validity to 1 November through 31 March. Lastly, SLICE is viable only in areas with greater than 95% sea ice concentration (SIC) due to the effects of open water on passive microwave emissivity. Based on the availability of CryoSat-2 data, the results cover 2010 through 2021 except November 2011 through March 2012, due to a gap in the passive microwave data coverage. The results are on a weekly basis following the temporal resolution of CS2SMOS but are shown here and in Anheuser et al. (2023a) on a monthly basis. The CS2SMOS and both thermodynamic and residual data are on the 25 km EASE-Grid 2.0, while the snow–ice interface temperature retrieval data is linearly interpolated from its north polar stereographic to match.

2.3. CESM2-OMIP2

NCAR CESM2 is a World Climate Research Program (WCRP) CMIP Phase 6 (Eyring et al., 2016) class, fully coupled Earth system model (Danabasoglu et al., 2020) consisting of biogeochemistry, atmosphere, land, ocean, and sea ice components. The CESM2-OMIP2 experiment served as the NCAR contribution to OMIP2, which was endorsed as part of CMIP6 (Eyring et al., 2016; Tsujino et al., 2020). This ocean and sea ice only model run utilizes the Parallel Ocean Program, version 2 ocean model (POP2) (Smith et al., 2010) and Los Alamos National Laboratory (LANL) Community Ice Code Version 5.1.2 sea ice model (CICE5) (Hunke et al., 2015). CICE5 includes the thermodynamics described by Bitz and Lipscomb (1999) and the dynamics described by Hunke and Dukowicz (2002), which incorporates an elastic-viscous-plastic sea ice rheology. The ice thickness distribution within each grid cell is described by Thorndike et al. (1975) and is discretized into eight categories. The CICE5 model includes a parameterization of multi-phase thermodynamics as described by Turner and Hunke (2015) and includes a melt pond parameterization (Hunke et al., 2013) and salinity dependent freezing temperature.

CESM2-OMIP2 is forced by an adapted version of the Japanese 55-year atmospheric reanalysis product (JRA-55) (Kobayashi et al., 2015), called JRA55-driving ocean (JRA55-do), that was purpose-built for driving ocean-sea ice models (Tsujino et al., 2018). As such, CESM2-OMIP2 is intended to mimic observed conditions. The single CESM2-OMIP2 simulation covers 1958 to 2018 and is spun up by repeating the 61 years forcing cycle five times prior to the sixth cycle. Here we used monthly data from this sixth cycle accessed via the Earth System Grid Federation (https://esgf.llnl.gov/index.html, last access: 10 October 2022). Basal thermodynamic growth is directly output while frazil, snow–ice and evaporation/sublimation thickness changes are also output and included in the residual category along with dynamics. Sea ice mass tendencies output by CESM2-OMIP2 were converted to thickness tendencies in m $month^{-1}$ using a density of 917 kg m^{-3} following Anheuser et al. (2022) and Alexandrov et al. (2010).

2.4. PIOMAS

Similar to CESM2-OMIP2, the Pan-Arctic Ice–Ocean Modeling and Assimilation System (PIOMAS) is a reanalysis-driven, coupled sea ice model. PIOMAS utilizes the POP ocean model version 1, coupled with a thickness and enthalpy distribution (TED) sea ice model (Zhang & Rothrock, 2003a). The TED model treats thickness as a discretized distribution using 12 categories with a ridging term (Thorndike et al., 1975) and includes a viscous–plastic rheology (Hibler, 1979). The output dataset is intended to replicate historical sea ice thickness from 1978 to the present and is created by driving the model using daily National Snow and Ice Data Center (NSIDC) SIC and NCEP/NCAR reanalysis surface forcing and sea surface temperatures (SSTs). Basal growth is the only thermodynamic process modeled so residual processes include only dynamics.

3. Method and Results

The thickness datasets were converted to m and tendency datasets to m $month^{-1}$. Results are November to March monthly mean data from each dataset including only grid cells with greater than 95% SIC. Comparisons begin November 2010 based on the availability of SLICE, and end after December 2018 with the end of CESM2-OMIP2. November 2011 through March 2012 is excluded due to the gap in SLICE availability. The PIOMAS and CESM2-OMIP2 datasets were linearly interpolated to the 25 km EASE-Grid 2.0.

Monthly mean thickness, basal thermodynamic growth and residual changes from CS2SMOS/SLICE, PIOMAS and OMIP2 are depicted in Figure 1 and uncertainties of the CS2SMOS/SLICE terms are shown in Figure S1 in Supporting Information S1. Figure 2 shows differences between CS2SMOS/SLICE and both PIOMAS and

10.1029/2023GL106963

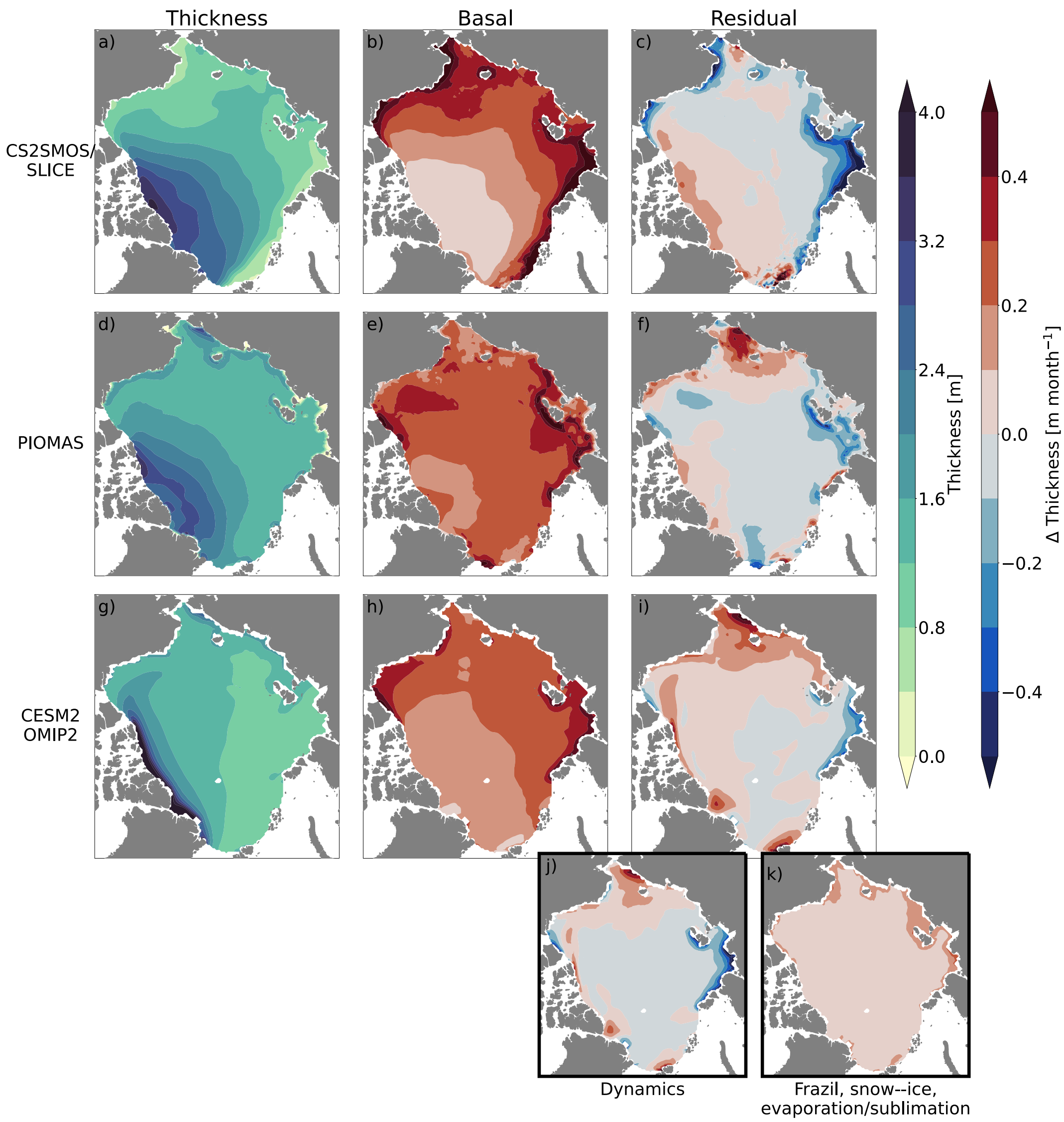

Figure 1. Monthly mean overall thickness, basal growth and residual thickness changes from November to March beginning with November 2010 and ending with December 2018 (excluding November 2011–March 2012) for CS2SMOS/SLICE (a–c), PIOMAS (d–f) and CESM2-OMIP2 (g–i). CESM OMIP2 residual effects are further partitioned into dynamics and frazil, snow–ice and evaporation/sublimation thickness changes (j–k). All datasets show high mean thickness and low basal thermodynamic growth near the Canadian Arctic Archipelago and low mean thickness and high basal thermodynamic growth in the peripheral seas, though CS2SMOS/SLICE show a larger magnitude and gradual gradient than PIOMAS or CESM2-OMIP2. Additionally, while basal growth is always positive, residual processes are positive in some regions and negative in others and serve to maintain the pattern in mean thickness.

CESM2-OMIP2 in these terms. Thermodynamic and residual effects are summed across the entire region and by regions per Meier and Stewart (2023) on a mean monthly volume basis in Figure 3 and as a time series in Figure S2 in Supporting Information S1.

All datasets show a mean thickness field in Figure 1 with the greatest values, near 4 m, north of the Canadian Arctic Archipelago (CAA) decreasing to the lowest values, near 1 m, in the peripheral seas. However, this decrease is more gradual, uniform and significant across the Arctic basin in CS2SMOS than in PIOMAS or CESM2-OMIP2. Of particular note is a narrow region of sea ice thickness, greater than 4 m, along the northern boundary of the CAA present in the CESM2-OMIP2 dataset but not in the others. Figure 2 shows these differences, with both CESM2-OMIP2 and PIOMAS having less ice thickness in the central Arctic and more ice thickness in the peripheral seas when compared to CS2SMOS. The differences

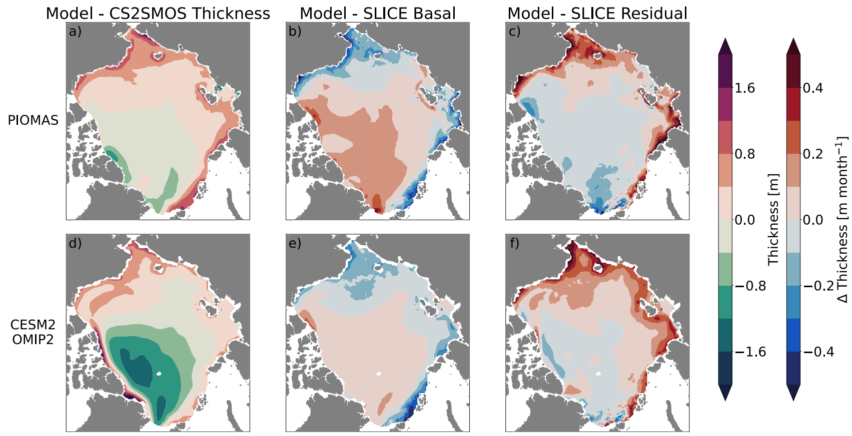

Figure 2. Monthly mean overall thickness, basal growth and residual thickness change differences between PIOMAS and CS2SMOS/SLICE (a–c), and CESM2-OMIP2 and CS2SMOS/SLICE (d–f) from November to March beginning with November 2010 and ending with December 2018 (excluding November 2011–March 2012). For both PIOMAS and CESM2-OMIP2, mean thickness and residual processes are negatively biased in the central Arctic and positively biased in the peripheral seas while basal thermodynamic growth differences show a reversed pattern of positive bias in the central Arctic and negative bias in the peripheral seas.

in the central Arctic are particularly strong in CESM2-OMIP2 where thickness is often lower than CS2SMOS by over 1 m with the exception of the narrow strip along the CAA, where thickness is higher by an even greater margin.

The basal thermodynamic growth fields all broadly show higher growth in the peripheral seas than the central Arctic, as expected due to the inverse relationship between thickness and growth rate. However, this pattern is more significant in SLICE than the others, following the corresponding effect in mean thickness fields. Over a large area between the CAA and the North Pole, SLICE depicts very low basal thermodynamic sea ice thickness growth, less than 0.1 m month^{-1}. Neither of the other two datasets show such a low basal thermodynamic growth anywhere across the study region. Over the central Arctic, the CESM2 mean ice thickness is 1 m thinner than that

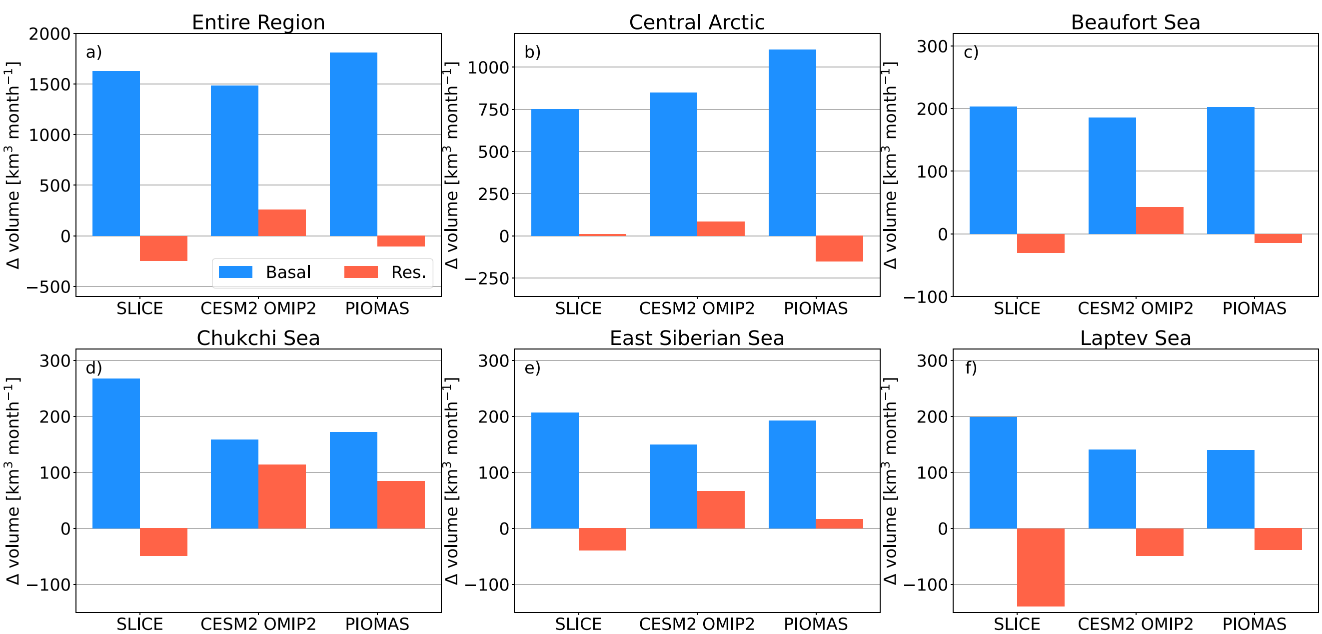

Figure 3. Basal growth (blue) and residual changes (orange) for SLICE, CESM2-OMIP2 and PIOMAS for the entire region (a), central Arctic (b), Beaufort Sea (c), Chukchi Sea (d), East Siberian Sea (e) and Laptev Sea (f) from November to March beginning with November 2010 and ending with December 2018 (excluding November 2011–March 2012). Over the entire region and peripheral seas, the models have greater dynamic effect than the observational estimates.

of SLICE and PIOMAS, however the sea ice thermodynamic growth is much closer to that of SLICE than PIOMAS. Basal thermodynamic growth in the peripheral seas are similar across the datasets, though the polynyas show increased basal thermodynamic growth in SLICE over the others. Additionally, PIOMAS and CESM2-OMIP2 have lower basal thermodynamic growth in the Chukchi and East Siberian Seas relative to SLICE and higher mean thickness relative to CS2SMOS. These patterns are confirmed in Figure 2, where lower basal thermodynamic growth in the peripheral seas of 0–0.1 m month^{-1} is mirrored by higher basal thermodynamic growth by a similar or, as in the PIOMAS data, greater margin in the central Arctic relative to the observational estimates.

Mean residual effects from the three datasets have similarities in Figure 1 but also subtle differences. In all datasets, residual effects contribute to thickness increases in some areas of the Chukchi and East Siberian Sea, likely due to ridging and advection of thicker ice into them (Duncan & Farrell, 2022), and decreases in coastal Laptev Seas, likely due to divergence of ice seaward from coastal polynyas (Hoffman et al., 2019; Willmes & Heinemann, 2016), but the extent and magnitude of these effects differ. In the SLICE dataset, residual effects rarely exceed 0.2 m month^{-1} in the Chukchi and East Siberian Seas, whereas both PIOMAS and CESM2-OMIP2 show much of this region exceeding 0.2 m month^{-1} and sometimes greater than 0.4 m month^{-1}. In the Laptev Sea, residual effects of less than −0.4 m month^{-1} are found in SLICE but rarely are less than −0.2 m month^{-1} in the other datasets.

An important difference between SLICE and both PIOMAS and CESM2-OMIP2 is a region of significant residual thickness increase found in SLICE just north of most of the CAA and extending towards the peripheral seas, between 0.1 m month^{-1} and 0.2 m month^{-1} (Figure 1), likely due to ridging and convergence by the Beaufort Gyre and Transpolar Drift (Duncan & Farrell, 2022; Kwok & Cunningham, 2016). Neither PIOMAS nor CESM2-OMIP2 depicts this region to be as expansive, though both show indications of this area and CESM2-OMIP2 includes a larger region of 0–0.1 month^{-1}. The CESM2-OMIP2 residual is also partitioned into the dynamics component and a frazil, snow–ice, evaporation/sublimation component, showing that dynamics dictates the residual effect pattern though the frazil, snow–ice and evaporation/sublimation component does contribute to thickness increase basin-wide. These trends are also depicted in Figure 2 showing modeled Central Arctic residual effects are lower than the observational estimates by 0–0.1 m month^{-1} and higher, sometimes by greater margins, in much of the remaining areas.

Figure 3 shows both basal thermodynamic growth and residual effects summed across the study region and each sub-region. Across the entire study region, PIOMAS shows the most basal thermodynamic growth and CESM2-OMIP2 the least. Mean residual effects have a net negative effect across the study region in SLICE and PIOMAS but are positive in CESM2-OMIP2, signally a significant deviation between the models. Confirming the trend discussed above, SLICE residual effects are below that of CESM2-OMIP2 and PIOMAS in the Chukchi, East Siberian and Laptev Seas. Curiously, Central Arctic basal thermodynamics are greatest in CESM2-OMIP2, likely owing to the regional boundary extending beyond the broad region of underestimated dynamics shown in Figure 2. Figure S2 shows this data in a yearly time series format. The datasets often show similar year to year variation in basal thermodynamic growth, particularly across the entire region, where all three datasets show similar magnitudes and variation. The same cannot be said for residual effects, where both yearly variation and magnitudes are often different amongst the datasets. It is difficult to discern any temporal trends during the CS2SMOS/SLICE time period.

SLICE is largely driven by the passive–microwave–retrieved snow–ice interface temperature. To add context to the comparison between SLICE and CESM2-OMIP2, differences between CESM2-OMIP2 and passive microwave snow–ice interface temperature as well as differences between SLICE and SLICE replicated using CESM2-OMIP2 snow–interface temperature and thickness are shown in Figure 4. The model has warmer snow–ice interface temperatures than the satellite retrieval over most of the study area, with the exception of a region of negative bias, less than 4 K, just north of the western CAA and in the Beaufort Sea. Over much of the remaining area, the difference is less than 4 K. In much of the eastern hemisphere, however, differences are between 4 and 8 K and sometimes greater. The resultant differences in SLICE and CESM2-OMIP2 SLICE-replica follow these trends. Thermodynamic growth from CESM2-OMIP2 SLICE-replica is reduced versus model output thermodynamic growth. Even still, the differences between CESM2-OMIP2 SLICE-replica and SLICE show a similar pattern to those shown in Figure 2 with higher basal growth in the central Arctic and lower basal growth in the peripheral seas compared to SLICE.

10.1029/2023GL106963

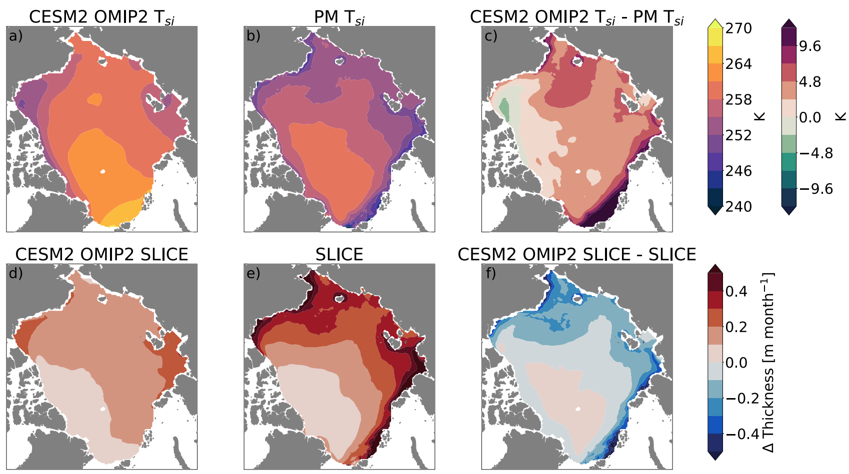

Figure 4. Mean CESM2-OMIP2 T_{si} (a), mean passive microwave T_{si} (b) and their difference (c) and mean CESM2-OMIP2 SLICE (d), mean SLICE (e) and their difference (f) from November to March beginning with November 2010 and ending with December 2018 (excluding November 2011–March 2012). Even though CESM2-OMIP2 snow–ice interface temperature is biased positive relative to passive microwave snow–ice interface temperature, CESM2-OMIP2 SLICE has a similar difference with SLICE of positive biased growth in the central Arctic and negative biased growth in the peripheral seas.

4. Discussion

Basal thermodynamic processes work to reduce spatial gradients in sea ice thickness via the inverse relationship between growth rate and thickness present in Equation 2, leaving residual processes to maintain large scale spatial structure in thickness patterns. Figures 1 and 2 show mean thickness structures in all datasets that closely reflect the structure in the residual effects. To better match mean thickness from CS2SMOS, the PIOMAS and CESM2 models would need to better reflect the residual effect patterns revealed by SLICE. In turn, representation of basal thermodynamic growth would more closely match SLICE via the influence of mean thickness on this process. Because the majority of residual effects are due to dynamics as the 95% SIC and wintertime-only constraints on this analysis minimizes the impact of thermodynamic processes outside of basal growth, adjustment to dynamic model components such that thickness increases that currently manifest in the Chukchi and East Siberian Seas were relocated to more expansive regions north of the CAA may improve model outputs.

Both models rely upon similar model strategies and utilize the same POP ocean model and are reanalysis-forced. Both models use a governing thickness equation as described by Thorndike et al. (1975). A momentum balance accounts for the various forces acting on sea ice and determines the ice motion field. Essential to this component of the models are a set of parameterizations that determine what results when a stress is applied to a parcel of ice. Does the ice move? Does the ice ridge and raft upon nearby ice? Does the ice break free of surrounding ice and form a lead? Does the ice remain in place and compress? It is possible that adjustments must be made in these processes for the models to more accurately reflect observational estimates of thermodynamic and residual effects. It is possible that the underlying ocean circulation needs to be adjusted to achieve these dynamic effects as well, especially given the both models use versions of the POP ocean model.

Differences in basal thermodynamic growth between SLICE and the models reflect the difference in overall thickness caused by dynamic processes but also may be affected by contrasts in how each dataset models thermodynamic processes. Whereas instantaneous retrieval of thermodynamic growth rate in SLICE is made possible by assuming a linear vertical temperature profile in the ice, PIOMAS and CESM2-OMIP2 discretize the ice–snow system into layers, allowing for variable profiles that account for thermal inertia. These effects are typically not significant in winter but may play a role in early and late growth season. PIOMAS and CESM2-OMIP2 account for radiative processes at the snow surface, albeit through reanalysis data that have known issues in the Arctic (Batrak & Müller, 2019). SLICE does not account for these radiative processes but need not do so because use of the snow–ice interface temperature as the upper boundary condition for the vertical profile removes the snow and surface radiative processes from the system. Consequently, SLICE is directly impacted by any errors in the snow–

ice interface temperature retrieval. Finally, SLICE treats thickness as constant throughout a grid cell, whereas both CESM2-OMIP2 and PIOMAS represent thickness as a distribution. Because the effect of thickness on growth rate is non-linear, this may affect the results.

Often, comparisons of sea ice thickness in global climate models to observations are avoided due to uncertainties in the observations. Figure S1 in Supporting Information S1 shows uncertainties in the mean fields in Figure 1. Differences between the observational estimates and model outputs shown in Figure 2 are greater in most regions than the uncertainty. These uncertainties were calculated using the methodology described in Anheuser et al. (2023a), which allows for a correlation coefficient of 0.6 between spatial and temporal neighbors in the calculation of uncertainties in the spatial and temporal derivatives of CS2SMOS that are present in the SLICE methodology. The rationale for the use of this coefficient and further discussion of SLICE uncertainty is found in Anheuser et al. (2023a). Other covariances may exist across the input sources to SLICE but are difficult to identify.

5. Summary

Observations of thermodynamic sea ice thickness growth and dynamic sea ice thickness effects based on satellite data (Anheuser et al., 2023a) make possible an examination of these processes as represented by a global climate model and a sea ice model reanalysis. Relative to these observational estimates, both CESM2-OMIP2 and PIOMAS exhibit a similar pattern of higher basal thermodynamic growth and lower residual effects in the central Arctic, and vice versa in the regions where the Transpolar Drift originates and the Chukchi, Barents and Kara Seas. That these datasets show similar results is not surprising, given that the sea ice model components within each are built upon the same fundamental studies and ocean model. It is likely that adjustments to the parameterization of the dynamic component of the sea ice models is required. This study is a first step towards understanding how climate models represent the processes that influence sea ice thickness and how these processes compare with current real world conditions in observational estimates.

Data Availability Statement

Code for creation of the figures in this work is available at Anheuser et al. (2023c). Observational estimate data described by Anheuser et al. (2023a) is available at Anheuser et al. (2023b). The production of the merged CryoSat-SMOS sea ice thickness data was funded by the ESA project SMOS & CryoSat-2 Sea Ice Data Product Processing and Dissemination Service (grant: REKLIM-2013-04), and data from 1 November 2010–1 December 2018 were obtained from the Alfred Wegener Institute (AWI) (Kaleschke et al., 2019). National Climate and Atmospheric Research (NCAR) Community Earth System Model 2 (CESM2) data was accessed via the Earth System Grid Federation (Danabasoglu, 2019). Pan-Arctic Ice-Ocean Modeling and Assimilation System (PIOMAS) data was accessed at Zhang and Rothrock (2003b).

Acknowledgments

This work was supported by the National Oceanic and Atmospheric Administration (Grant NA20NES4320003). The views, opinions, and findings contained in this report are those of the authors and should not be construed as an official National Oceanic and Atmospheric Administration or U.S. Government position, policy, or decision.

References

Alexandrov, V., Sandven, S., Wahlin, J., & Johannessen, O. M. (2010). The relation between sea ice thickness and freeboard in the Arctic. *The Cryosphere*, *4*(3), 373–380. https://doi.org/10.5194/tc-4-373-2010

Anheuser, J., Liu, Y., & Key, J. (2022). A simple model for daily basin-wide thermodynamic sea ice thickness growth retrieval. *The Cryosphere*, *16*(10), 4403–4421. https://doi.org/10.5194/tc-16-4403-2022

Anheuser, J., Liu, Y., & Key, J. R. (2023a). A climatology of thermodynamic vs. dynamic Arctic wintertime sea ice thickness effects during the CryoSat-2 era. *The Cryosphere*, *17*(7), 2871–2889. https://doi.org/10.5194/tc-17-2871-2023

Anheuser, J., Liu, Y., & Key, J. R. (2023b). A climatology of thermodynamic vs. dynamic Arctic wintertime sea ice thickness effects during the CryoSat-2 era: Data (3.0.0). [Dataset]. Zenodo. https://doi.org/10.5281/zenodo.7987917

Anheuser, J., Liu, Y., & Key, J. R. (2023c). janheuser/modcomp: 2.0.0 [Software]. Zenodo. https://doi.org/10.5281/zenodo.10431789

Arthun, M., Onarheim, I. H., Dorr, J., & Eldevik, T. (2021). The seasonal and regional transition to an ice-free Arctic. *Geophysical Research Letters*, *48*(1). https://doi.org/10.1029/2020gl090825

Arzel, O., Fichefet, T., & Goosse, H. (2006). Sea ice evolution over the 20th and 21st centuries as simulated by current AOGCMs. *Ocean Modelling*, *12*(3–4), 401–415. https://doi.org/10.1016/j.ocemod.2005.08.002

Batrak, Y., & Müller, M. (2019). On the warm bias in atmospheric reanalyses induced by the missing snow over arctic sea-ice. *Nature Communications*, *10*(4170), 4170. https://doi.org/10.1038/s41467-019-11975-3

Bitz, C. M., & Lipscomb, W. H. (1999). An energy-conserving thermodynamic model of sea ice. *Journal of Geophysical Research-Oceans*, *104*(C7), 15669–15677. https://doi.org/10.1029/1999jc900100

Boe, J. L., Hall, A., & Qu, X. (2009). sea-ice cover in the Arctic Ocean projected to vanish by 2100. *Nature Geoscience*, *2*(5), 341–343. https://doi.org/10.1038/ngeo467

Danabasoglu, G. (2019). NCAR CESM2 model output prepared for CMIP6 OMIP omip2. [Dataset]. Earth System Grid Federation. https://doi.org/10.22033/ESGF/CMIP6.7680

Danabasoglu, G., Lamarque, J. F., Bacmeister, J., Bailey, D. A., DuVivier, A. K., Edwards, J., et al. (2020). The Community Earth System Model version 2 (CESM2). *Journal of Advances in Modeling Earth Systems*, *12*(2). https://doi.org/10.1029/2019ms001916

Duncan, K., & Farrell, S. L. (2022). Determining variability in Arctic sea ice pressure ridge topography with ICESat-2. *Geophysical Research Letters*, *49*(18), e2022GL100272. https://doi.org/10.1029/2022GL100272

Eyring, V., Bony, S., Meehl, G. A., Senior, C. A., Stevens, B., Stouffer, R. J., & Taylor, K. E. (2016). Overview of the Coupled Model Intercomparison Project phase 6 (CMIP6) experimental design and organization. *Geoscientific Model Development*, *9*(5), 1937–1958. https://doi.org/10.5194/gmd-9-1937-2016

Feltham, D. L., Untersteiner, N., Wettlaufer, J. S., & Worster, M. G. (2006). Sea ice is a mushy layer. *Geophysical Research Letters*, *33*(14), L14501. https://doi.org/10.1029/2006gl026290

Flato, G., & Participating CMIP Modelling Groups (2004). Sea-ice and its response to CO2 forcing as simulated by global climate models. *Climate Dynamics*, *23*(3–4), 229–241. https://doi.org/10.1007/s00382-004-0436-7

Hibler, W. D. (1979). Dynamic thermodynamic sea ice model. *Journal of Physical Oceanography*, *9*(4), 815–846. https://doi.org/10.1175/1520-0485(1979)0090815:adtsim2.0.co;2

Hibler, W. D. (1980). Modeling a variable thickness sea ice cover. *Monthly Weather Review*, *108*(12), 1943–1973. https://doi.org/10.1175/1520-0493(1980)1081943:mavtsi2.0.co;2

Hoffman, J. P., Ackerman, S. A., Liu, Y. H., & Key, J. R. (2019). The detection and characterization of Arctic sea ice leads with satellite imagers. *Remote Sensing*, *11*(5), 521. https://doi.org/10.3390/rs11050521

Holland, M. M., Serreze, M. C., & Stroeve, J. (2010). The sea ice mass budget of the Arctic and its future change as simulated by coupled climate models. *Climate Dynamics*, *34*(2–3), 185–200. https://doi.org/10.1007/s00382-008-0493-4

Hunke, E. C., & Dukowicz, J. K. (2002). The elastic-viscous-plastic sea ice dynamics model in general orthogonal curvilinear coordinates on a sphere-incorporation of metric terms. *Monthly Weather Review*, *130*(7), 1848–1865. https://doi.org/10.1175/1520-0493(2002)1301848:tevpsi2.0.co;2

Hunke, E. C., Hebert, D. A., & Lecomte, O. (2013). Level-ice melt ponds in the Los Alamos sea ice model, CICE. *Ocean Modelling*, *71*, 26–42. https://doi.org/10.1016/j.ocemod.2012.11.008

Hunke, E. C., Lipscomb, W. H., Turner, A. K., Jeffery, N., & Elliott, S. (2015). CICE: The Los Alamos sea ice model documentation and software user's manual version 5.1, LA-CC-06-012. Retrieved from http://www.ccpo.odu.edu/~klinck/Reprints/PDF/cicedoc2015.pdf

Kaleschke, L., Hendricks, S., Tian-Kunze, X., & Ricker, R. (2019). CryoSat-SMOS Merged Sea Ice Thickness, Version 205. [Dataset]. https://spaces.awi.de/display/CS2SMOS/CryoSat-SMOS+Merged+Sea+Ice+Thickness

Keen, A., Blockley, E., Bailey, D. A., Debernard, J. B., Bushuk, M., Delhaye, S., et al. (2021). An inter-comparison of the mass budget of the Arctic sea ice in CMIP6 models. *The Cryosphere*, *15*(2), 951–982. https://doi.org/10.5194/tc-15-951-2021

Kilic, L., Tonboe, R. T., Prigent, C., & Heygster, G. (2019). Estimating the snow depth, the snow–ice interface temperature, and the effective temperature of Arctic sea ice using Advanced Microwave Scanning Radiometer 2 and ice mass balance buoy data. *The Cryosphere*, *13*(4), 1283–1296. https://doi.org/10.5194/tc-13-1283-2019

Kobayashi, S., Ota, Y., Harada, Y., Ebita, A., Moriya, M., Onoda, H., et al. (2015). The JRA-55 reanalysis: General specifications and basic characteristics. *Journal of the Meteorological Society of Japan*, *93*(1), 5–48. https://doi.org/10.2151/jmsj.2015-001

Kwok, R., & Cunningham, G. F. (2016). Contributions of growth and deformation to monthly variability in sea ice thickness north of the coasts of Greenland and the Canadian Arctic Archipelago. *Geophysical Research Letters*, *43*(15), 8097–8105. https://doi.org/10.1002/2016gl069333

Laxon, S. W., Giles, K. A., Ridout, A. L., Wingham, D. J., Willatt, R., Cullen, R., et al. (2013). Cryosat-2 estimates of Arctic sea ice thickness and volume. *Geophysical Research Letters*, *40*(4), 732–737. https://doi.org/10.1002/grl.50193

Lebrun, M., Vancoppenolle, M., Madec, G., & Massonnet, F. (2019). Arctic sea-ice-free season projected to extend into autumn. *The Cryosphere*, *13*(1), 79–96. https://doi.org/10.5194/tc-13-79-2019

Lepparanta, M. (1993). A review of analytical models of sea–ice growth. *Atmosphere-Ocean*, *31*(1), 123–138. https://doi.org/10.1080/07055900.1993.9649465

Massonnet, F., Fichefet, T., Goosse, H., Bitz, C. M., Philippon-Berthier, G., Holland, M. M., & Barriat, P. Y. (2012). Constraining projections of summer Arctic sea ice. *The Cryosphere*, *6*(6), 1383–1394. https://doi.org/10.5194/tc-6-1383-2012

Meier, W. N., & Stewart, J. S. (2023). *Arctic and antarctic regional masks for sea ice and related data products, version 1*. National Snow and Ice Data Center. https://doi.org/10.5067/CYW3O8ZUNIWC

Notz, D., Dorr, J., Bailey, D. A., Blockley, E., Bushuk, M., Debernard, J. B., & Community, S. (2020). Arctic sea ice in CMIP6. *Geophysical Research Letters*, *47*(10), 11. https://doi.org/10.1029/2019gl086749

Ricker, R., Hendricks, S., Kaleschke, L., Tian-Kunze, X., King, J., & Haas, C. (2017). A weekly Arctic sea-ice thickness data record from merged CryoSat-2 and SMOS satellite data. *The Cryosphere*, *11*(4), 1607–1623. https://doi.org/10.5194/tc-11-1607-2017

Shu, Q., Song, Z., & Qiao, F. (2015). Assessment of sea ice simulations in the CMIP5 models. *The Cryosphere*, *9*(1), 399–409. https://doi.org/10.5194/tc-9-399-2015

Shu, Q., Wang, Q., Song, Z. Y., Qiao, F. L., Zhao, J. C., Chu, M., & Li, X. F. (2020). Assessment of sea ice extent in CMIP6 with comparison to observations and CMIP5. *Geophysical Research Letters*, *47*(9). https://doi.org/10.1029/2020gl087965

Smith, L. C., & Stephenson, S. R. (2013). New trans-Arctic shipping routes navigable by midcentury. *Proceedings of the National Academy of Sciences of the United States of America*, *110*(13), E1191–E1195. https://doi.org/10.1073/pnas.1214212110

Smith, R., Jones, P., Briegleb, B., Bryan, F., Danabasoglu, G., Dennis, J., et al. (2010). The parallel ocean program (POP) reference manual: Ocean component of the community climate system model (CCSM) and Community Earth System Model (CESM), LAUR-10-01853. Retrieved from https://www2.cesm.ucar.edu/models/cesm1.2/pop2/doc/sci/POPRefManual.pdf

Stefan, J. (1891). Ueber die theorie der eisbildung, insbesondere über die eisbildung im polarmeere. *Annalen der Physik-Berlin*, *278*(2), 269–286. https://doi.org/10.1002/andp.18912780206

Stroeve, J., Holland, M. M., Meier, W., Scambos, T., & Serreze, M. (2007). Arctic sea ice decline: Faster than forecast. *Geophysical Research Letters*, *34*(9). https://doi.org/10.1029/2007gl029703

Thorndike, A. S., Rothrock, D. A., Maykut, G. A., & Colony, R. (1975). Thickness distribution of sea ice. *J. Geophys. Res.-Oc. Atm.*, *80*(33), 4501–4513. https://doi.org/10.1029/JC080i033p04501

Tsujino, H., Urakawa, L. S., Griffies, S. M., Danabasoglu, G., Adcroft, A. J., Amaral, A. E., et al. (2020). Evaluation of global ocean-sea-ice model simulations based on the experimental protocols of the Ocean Model Intercomparison Project phase 2 (OMIP-2). *Geoscientific Model Development*, *13*(8), 3643–3708. https://doi.org/10.5194/gmd-13-3643-2020

Tsujino, H., Urakawa, S., Nakano, H., Small, R. J., Kim, W. M., Yeager, S. G., et al. (2018). JRA-55 based surface dataset for driving ocean-sea-ice models (JRA55-do). *Ocean Modelling*, *130*, 79–139. https://doi.org/10.1016/j.ocemod.2018.07.002

10.1029/2023GL106963

Turner, A. K., & Hunke, E. C. (2015). Impacts of a mushy-layer thermodynamic approach in global sea-ice simulations using the CICE sea-ice model. *Journal of Geophysical Research-Oceans*, *120*(2), 1253–1275. https://doi.org/10.1002/2014jc010358

Wang, M. Y., & Overland, J. E. (2015). Projected future duration of the sea-ice-free season in the Alaskan Arctic. *Progress in Oceanography*, *136*, 50–59. https://doi.org/10.1016/j.pocean.2015.01.001

Willmes, S., & Heinemann, G. (2016). Sea-ice wintertime lead frequencies and regional characteristics in the Arctic, 2003-2015. *Remote Sensing*, *8*(1), 4. https://doi.org/10.3390/rs8010004

Wingham, D. J., Francis, C. R., Baker, S., Bouzinac, C., Brockley, D., Cullen, R., et al. (2006). CryoSat: A mission to determine the fluctuations in Earth's land and marine ice fields. *Natural Hazards and Oceanographic Processes from Satellite Data*, *37*(4), 841–871. https://doi.org/10.1016/j.asr.2005.07.027

Zhang, J., & Rothrock, D. (2003a). Modeling global sea ice with a thickness and enthalpy distribution model in generalized curvilinear coordinates. *Monthly Weather Review*, *131*(5), 845–861. https://doi.org/10.1175/1520-0493(2003)1310845:mgsiwa2.0.co;2

Zhang, J., & Rothrock, D. (2003b). PIOMAS variables on Model Grid, Version 2.1. [Dataset]. https://psc.apl.uw.edu/research/projects/arctic-sea-ice-volume-anomaly/data/model_grid

Zhang, J. L., & Rothrock, D. (2001). A thickness and enthalpy distribution sea-ice model. *Journal of Physical Oceanography*, *31*(10), 2986–3001. https://doi.org/10.1175/1520-0485(2001)0312986:ataeds2.0.co;2